Colossal Magnetoresistance in $La_{0.7}Ca_{0.3}MnO_{3-\delta}$: Comparative Study of Single-Crystal and Polycrystalline Material

Chang Seop Hong,† Wan Seop Kim,† Eun Ok Chi,† Kyu Won Lee,‡ and Nam Hwi Hur*,†

Center for CMR Materials, and Superconductivity Laboratory, Korea Research Institute of Standards and Science, Yusong, P.O. Box 102, Taejon 305-600, Korea

Received May 12, 2000. Revised Manuscript Received August 21, 2000

The magnetoresistance (MR) and transport properties of both single-crystal and polycrystalline samples of $La_{0.7}Ca_{0.3}MnO_{3-\delta}$ (LCMO) have been investigated to elucidate their magneto transport behaviors near and below the Curie temperature T_C. We find that negative MR is heavily dependent upon the surface morphology in the low-temperature, ferromagnetic regime. The polycrystalline sample postannealed at 1400 °C under the oxygen atmosphere exhibits large low-field MR in the whole temperature range below T_C, which is about 20% at 0.5 T. On the other hand, the single-crystal sample shows the remarkable suppression of resistivity only at the narrow temperature region near T_C. We suggest that the MR found in the polycrystalline sample is dominated by the tunneling of spin-polarized electrons between grains below T_C while the MR in the single crystal is mainly ascribed to the suppression of spin fluctuation. The difference in the MR property between the single-crystal and polycrystalline samples is discussed in terms of oxygen inhomogeneity and granular effects affected by interfacial melting.

Introduction

The recent interest in the perovskite-based manganese oxides, $Ln_{1-x}A_xMnO_3$, where Ln is a trivalent lanthanide ion and A is a divalent alkaline earth ion, has been motivated by the observation of colossal magnetoresistance (CMR) in these materials.[1−3] The fundamental mechanism of the CMR phenomenon is generally understood on the basis of the double-exchange (DE) theory in that electron hopping between the Mn^{3+} and Mn^{4+} pairs is facilitated only when the spins of the d electrons are aligned in parallel.[4] This DE model was successful in explaining qualitatively both the sharp resistivity drop and the observed large MR near the Curie temperature (T_C). However, there have been a growing number of theoretical and experimental studies for which the DE model alone cannot explain the complex magnetic properties of the manganite materials quantitatively.[5] From the DE theory, the MR should be correlated with the reduction of spin fluctuation by an applied magnetic field. In other words, it reaches maximum near T_C and reduces continuously with decreasing temperature below T_C. Unlike this expectation, a wide variety of field dependence on the MR, depending on the microstructural nature, has been reported. For instance, Hwang et al. found the large low-field MR that is nearly temperature independent below T_C for a polycrystalline $La_{2/3}Sr_{1/3}MnO_3$ sample.[6] They reveal that the low-field MR in polycrystalline material is dominated by the spin-polarized tunneling across the grain boundaries. More recently, Balcells et al. reported the low-field and high-field MR of polycrystalline $La_{2/3}Sr_{1/3}MnO_3$ materials with different grain sizes, also revealing that the MR is heavily dependent on the grain size below T_C but is almost independent of the grain size near T_C.[7] From a practical standpoint, the large low-field MR over a wide range of temperatures is desirable for device applications.

Despite extensive studies on the $La_{1-x}Sr_xMnO_3$ material, little is known on the MR at interfaces of the corresponding calcium analogues, $La_{1-x}Ca_xMnO_3$, to date by direct comparison of the magnetic and transport data on the single crystal with its polycrystalline congener. This is partly due to the difficulty in growing a single crystal of $La_{1-x}Ca_xMnO_3$. To elucidate the grain boundary effect on the MR below T_C in the $La_{1-x}Ca_x$-MnO_3 system, we have grown a single crystal of the $La_{0.7}Ca_{0.3}MnO_{3-\delta}$ material using the floating zone

* To whom correspondence should be addressed. E-mail: nhhur@kriss.re.kr.
† Center for CMR Materials.
‡ Superconductivity Laboratory.

(1) Jin, S.; Tiefel, T. H.; McCormack, M.; Fastnacht, R. A.; Ramesh, R.; Chel, H. *Science* **1994**, *264*, 413.
(2) Von Helmolt, R.; Wecker, J.; Holzapfel, B.; Schultz, L.; Samwer, K. *Phys. Rev. Lett.* **1993**, *71*, 2331.
(3) Rao, C. N. R.; Cheetham, A. K.; Mahesh, R. *Chem. Mater.* **1996**, *8*, 2421.
(4) Zener, C. *Phys. Rev.* **1951**, *82*, 403; Goodenough, J. B. *Phys. Rev.* **1995**, *100*, 564. Wollan, E. O.; Koehler, W. C. *Phys. Rev.* **1955**, *100*, 545.
(5) Millis, A. J.; Littlewood, P. B.; Shraiman, B. I. *Phys. Rev. Lett.* **1995**, *74*, 5144. Argyriou, D. N.; Mitchell, J. F.; Potter, C. D.; Hinks, D. G.; Jorgensen, J. D.; Balder, S. D. *Phys. Rev. Lett.* **1996**, *76*, 3826. Kim, K. H.; Jung, J. H.; Noh, T. W. *Phys. Rev. Lett.* **1998**, *81*, 1517.
(6) Hwang, H. Y.; Cheong, S.-W.; Ong, N. P.; Batlogg, B. *Phys. Rev. Lett.* **1996**, *77*, 2041.
(7) Balcells, L.; Fontcuberta, J.; Martínez, B.; Obradors, X. *Phys. Rev.* **1998**, *B58*, R14679.

10.1021/cm0003931 CCC: $19.00
Published on Web 11/02/2000

method.[8] Its structural, magnetic, and transport properties were investigated and compared with those of polycrystalline $La_{0.7}Ca_{0.3}MnO_{3-\delta}$ samples. In this paper we present the structural, magnetic, and magneto transport properties of the $La_{0.7}Ca_{0.3}MnO_{3-\delta}$ samples. The polycrystalline samples are postannealed in air or oxygen atmospheres to explore the granular effects on the conduction process. An interesting feature is that the postannealing plays an essential role in the transport property of the polycrystalline sample by giving rise to interfacial melting between grains and homogenizing oxygen inhomogeneity. The negative low-field MR observed in this material is ascribed to the tunneling of spin-polarized electrons between grains. In contrast, the MR of the single crystal is large near the T_C up to 97% at 5 T but does not yield any noticeable change in the ferromagnetic regime below T_C. This is mainly due to the absence of grains in the single crystal.

Experimental Section

The polycrystalline $La_{0.7}Ca_{0.3}MnO_{3-\delta}$ sample was prepared through a conventional solid-state synthesis technique. A stoichiometric mixture of La_2O_3, $CaCO_3$, and $MnCO_3$ was ground, pelletized, and calcined at 1000 °C for 20 h. Sintering was carried out in air at 1300 °C for 80 h with intermediate regrinding. La_2O_3 was completely dried at 1000 °C for 10 h prior to use and handled inside the argon-filled drybox. The as-prepared product denoted as LCMOP was obtained by final sintering at 1350 °C for 24 h in air. The oxygen-annealed sample ($LCMOO_2$) was prepared by oxygen annealing of the LCMOP pellet at 1400 °C for 24 h. All polycrystalline samples were slowly cooled to room temperature in a furnace, which usually takes about 8 h.

A single crystal of $La_{0.7}Ca_{0.3}MnO_{3-\delta}$ was grown using the floating zone method. The bulk material for crystal growth with the same nominal composition was prepared by using the solid-state reaction method. The resulting powder was ground and cold-pressed to a cylindrical shape with a diameter of 6 mm and a length of 80 mm. The feed rod was treated at 1300 °C for 20 h in air. The crystal growth apparatus (Crystal Systems Inc.) is an infrared radiation convergence type image furnace that consists of four mirrors and four halogen lamps. The input power for the halogen lamp is 1000 W, suitable for the growth of a $La_{0.7}Ca_{0.3}MnO_{3-\delta}$ crystal. The temperature of the image furnace was measured by detecting blackbody radiation of a graphite rod with a pyrometer. The melting temperature of $La_{0.7}Ca_{0.3}MnO_{3-\delta}$ is estimated to be about 1900 °C. Both feed and seed rods are coaxially in the center of a silica tube but rotated in opposite directions at a rate of 25 rpm. The growth rate is 2−3 mm/h and the oxygen flowing rate is 2.5 L/min. Some of the grown crystals were ground, pelletized, and annealed at 1400 °C for 20 h in air. The resulting sintered sample is denoted as LCMOSP.

X-ray powder diffraction (XRD) data were collected on a Rigaku RAD diffractometer using Cu Kα radiation with the power of 3 kW. Rietveld analysis using the FULLPROF program[9] was performed within the 2θ range 20°−100°. The oxygen content was determined by iodometric titration. The cation compositions of the single crystal were checked by electron-probe microanalysis using an electron microscope. The scanning electron microscopy (JEOL6400) was employed to examine the surface morphology. Magnetic and transport data were measured on a Quantum Design MPMS-5 SQUID magnetometer or a PPMS-7 magnetometer. Electrical resistivity measurements were carried out using a standard four-probe method with the current perpendicular to the applied magnetic field. Electrical contacts were made with silver paint.

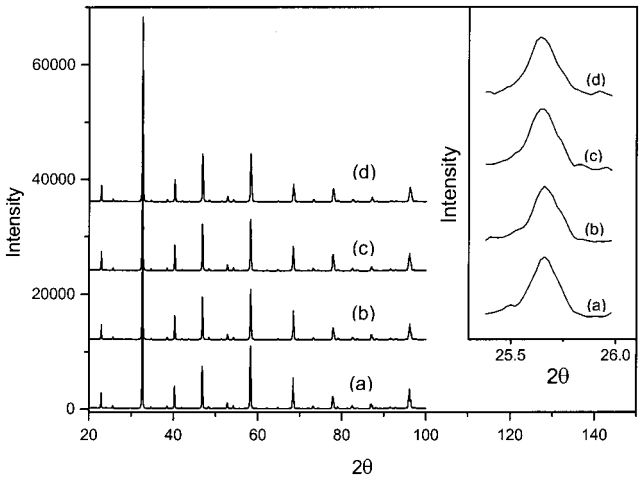

Figure 1. Power X-ray diffraction spectra of (a) LCMOP, (b) $LCMOO_2$, (c) LCMOSP, and (d) single crystal. The inset represents the expanded view of (111) diffraction peaks for all four samples.

Results and Discussion

In addition to the as-prepared $La_{0.7}Ca_{0.3}MnO_{3-\delta}$ sample (LCMOP), two polycrystalline samples with different annealing conditions were prepared and studied to compare the effects of grain size and interconnectivity between grains on the MR with those of a single crystal. One is the oxygen-annealed sample ($LCMOO_2$) prepared by postannealing of the LCMOP under the oxygen atmosphere. The other one (LCMOSP) was obtained from annealing of the ground single crystal as described in the Experimental Section. Interestingly, all the samples have almost identical oxygen contents determined by iodometric titration, which are estimated to be about 2.99 ± 0.01. They are very close to the nominal composition regardless of the synthetic pathway, suggesting that the sintering process does not significantly alter the oxygen stoichiometry. This result is consistent with previous work, in that to remove the oxygen in the $La_{1-x}Ca_xMnO_3$ sample with the optimal doping level ($x \sim 0.3$), a strong reducing agent such as a titanium getter is necessary.[10]

The XRD data of three polycrystalline samples and the single crystal that were obtained after grinding are shown in Figure 1. The XRD patterns are virtually identical to each other with a very small variation of 2θ values. They are indexed on the orthorhombic symmetry (space group: *Pnma*). Their lattice parameters obtained from the Rietveld profile analyses are summarized in Table 1. The refinement results show a slight change in their unit cell volumes, which is partly due to the annealing effect. This illustrates that the microstuctural changes occur in the materials by annealing, which is likely responsible for grain size variation as well as oxygen homogeneity. An attempt was made to determine the crystallite size by taking into account the William−Hall plot that correlates the measured XRD peak widths with the average grain

(8) Yi, H.; Hong, C. S.; Hur, N. H. *Solid State Commun.* **2000**, *114*, 579.

(9) Roisnel, T.; Rodríguez-Carvajal, J. *Program: Fullprof*; LLB-LCSIM, France, March 2000.

(10) Ju, H. L.; Gopalakrishana, J.; Peng, J. L.; Li, Q.; Xiong, G. C.; Venkatesan, T.; Greene, R. L. *Phys. Rev.* **1995**, *B51*, 6143.

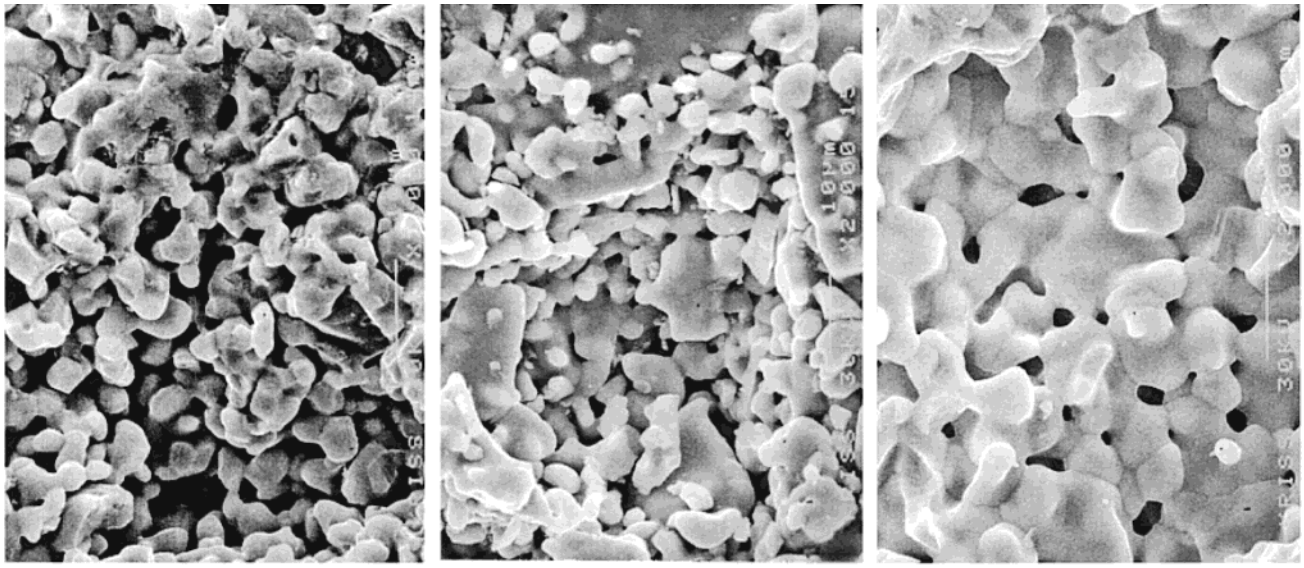

Figure 2. Scanning electron micrographs of (a) LCMOP, (b) LCMOSP, and (c) $LCMOO_2$.

Table 1. Lattice Parameters and Unit Cell Volumes Determined from Refinements of the X-ray Diffraction Data

sample	LCMOP	$LCMOO_2$	LCMOSP	single crystal
a (Å)	5.4788(1)	5.4766(2)	5.4793(1)	5.4762(4)
b (Å)	7.7432(1)	7.7397(2)	7.7447(2)	7.7373(4)
c (Å)	5.4926(1)	5.4907(2)	5.4944(1)	5.4881(3)
V (Å^3)	233.02(1)	232.74(1)	233.16(1)	232.54(2)
R_p (%)	8.62	7.72	8.11	6.66
R_{wp} (%)	10.9	10.5	10.5	9.16

size.[11] However, the fwhm's (full widths at half-maximum) and positions of the (111) peaks for all four samples are almost identical as shown in the inset of Figure 1. This suggests that these XRD data do not reflect noticeably the variation of the crystallite size.

To examine the microstructural change in more detail, we take the SEM (scanning electron microscopy) micrographs. Figure 2a−c shows the SEM morphologies for the LCMOP, LCMOSP, and $LCMOO_2$ samples, respectively. Unlike the XRD results, the SEM images clearly reveal the microstructural discrepancies between three samples. As can be seen in the SEM picture for LCMOP shown in Figure 2a, the as-prepared sample is slightly porous with a small grain size of about 3 μm. Obviously, this sample tends to have grain boundaries with weak links. The SEM image of LCMOSP displays partial melting and nonmelting regions with various grain sizes. In contrast, the oxygen-annealed sample ($LCMOO_2$) clearly exhibits large grains (average grain diameter: $\sim$5 μm) and better connectivity with overall interfacial melting in its SEM micrograph. It is interesting to note that this subtle difference in the surface structure directly reflects the transport property that will be discussed below.

The temperature-dependent magnetization data for the polycrystalline and pure single-crystalline samples are shown in Figure 3. The single crystal exhibits a sharp ferromagnetic transition with a T_C of 227 K. Its saturated magnetization value is 3.58 μ_B at 5 K, which is in good accord with the value for full alignment of the Mn spins, 3.7 μ_B. Other three polycrystalline samples also show the ferromagnetic transitions near that temperature. However, the transitions are less steep and the saturated magnetization values are smaller than that of the single crystal. The inset shows that the magnitudes and shapes of the d*M*/d*T* curves are varied depending on the sample quality, which renders some indications regarding the sample homogeneity. As can be seen clearly in the d*M*/d*T* curves, the single crystal has the sharpest transition. On the other hand, all the other samples display rather broad peaks, which is presumably due to the existence of grains.[12] Particularly, the two peaks in the ferromagnetic transition observed in LCMOP and LCMOSP implicates that there exist more than one ferromagnetic phase in the polycrystalline samples. A probable cause for the broad transition is the oxygen inhomogeneity where the upper peak can arise from an oxygen-rich, in other words hole-rich, region and the lower from an oxygen-poor (hole-poor) region relatively.[13] The steep transition and slight increase in T_C in $LCMOO_2$ are associated with the enhancement of grain size and oxygen incorporation by the postannealing under the oxygen atmosphere, which is consistent with the conclusion of earlier studies on the $La_{1-x}Ca_xMnO_3$ film.[14,15]

The temperature-dependent transport data for the polycrystalline and single-crystal samples are illustrated in the top panel of Figure 4, which is well correlated with the magnetization results displayed in Figure 3. As shown in the ρ−T curves, the resistivity data largely rely on the surface morphology and quality of the sample. The resistivity of the single crystal is at least 2 orders of magnitude smaller than the corre-

(11) Williamson, G. K.; Hall, W. H. *Acta Metall.* **1953**, *1*, 22. Woodward, P. M.; Cox, D. E.; Vogt, T. Rao, C. N. R.; Cheetham, A. K. *Chem. Mater.* **1999**, *11*, 3528.

(12) Zhang, N.; Ding, W.; Zhang, W.; Xing, D.; Du, Y. *Phys. Rev.* **1997**, *B56*, 8138.

(13) Sun, J. R.; Rao, G. H.; Zhang, Y. Z. *Appl. Phys. Lett.* 1998, *72*, 3208. Moreo, A.; Yonoki, S.; Dagotto, E. *Science* **1999**, *283*, 2034.

(14) Prellier, W.; Rajeswari, M.; Venkatesan, T.; Greene, R. L. *Appl. Phys. Lett.* **1999**, *75*, 1446.

(15) Nam, B. C.; Kim, W. S.; Choi, H. S.; Kim, J. C.; Hur, N. H.; Kim, I. S.; Park, Y. K. *J. Phys. D: Appl. Phys.*, in press.

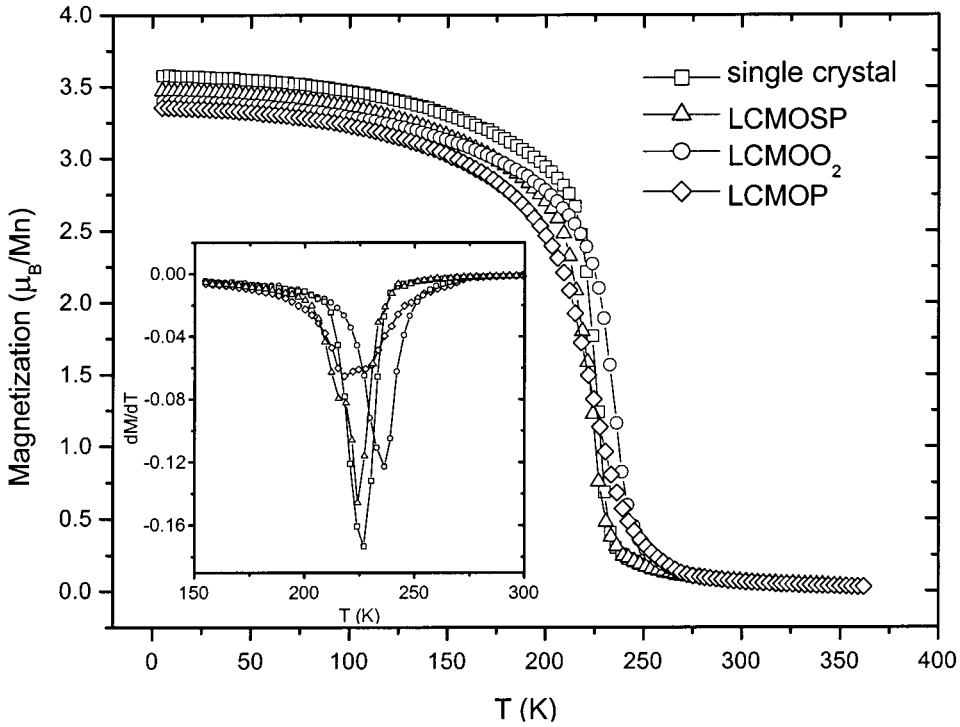

Figure 3. Temperature dependence of magnetization for the single-crystal and polycrystalline samples in a field of 0.5 T. The inset shows the temperature dependence of the differential magnetization (d*M*/d*T*).

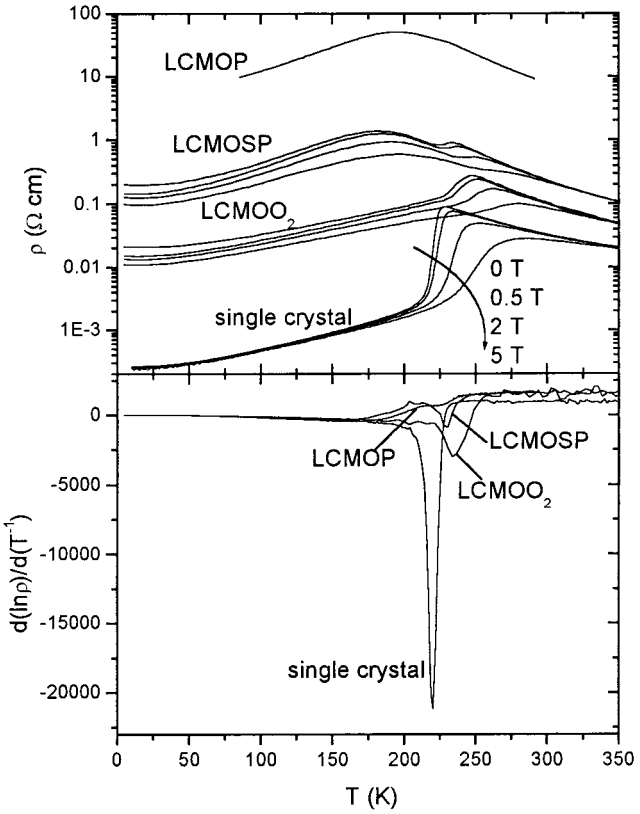

Figure 4. Top panel shows the temperature dependence of resistivity for $LCMOO_2$, LCMOSP, and a single crystal at various fields up to 5 T and the zero-field resistivity for LCMOP. Temperature dependence of the activation energy [≡d(ln ρ)/d(T^{-1})] is presented in the bottom panel.

sponding polycrystalline materials, indicating that the crystal has a dense and grain-free surface. Two distinctive transition peaks in LCMOP and LCMOSP in tune with their double magnetic transitions indicate that there exist two different percolative phases associated with the oxygen inhomogeneity. LCMOSP would give prominent evidence of grain boundary effects because the sample was synthesized directly by pulverizing pressed crystallites obtained from the single crystal that has only one peak near T_C. In other words, the transformation of a single crystal to a polycrystalline material leads to the formation of a grain boundary, possibly conferring complex features on transport properties. The grain boundary obviously influences the mobility of itinerant electrons in the polycrystalline samples and probably lifts the overall background in the resistivity curve.

From the activation energy [≡d(ln ρ)/d(T^{-1})] versus T curves presented in the bottom panel of Figure 4, the single crystal shows a distinctive sharp metal−insulator (M−I) transition but all three polycrystalline sample exhibit rather broad M−I transitions. These results are consistent with the microstructural changes and magnetization data described previously. The postannealing of the sample under the oxygen atmosphere drastically moves this broad transition to a single peak at higher temperature as can be seen in the $\rho-T$ curve of $LCMOO_2$. At this stage, it would be interesting to argue the influence of postannealing under oxygen on electrical conduction routes by the comparison between LCMOP and $LCMOO_2$. First, the postannealing at elevated temperature provides interfacial melting, leading to a more favorable percolative pathway for mobile electrons in $LCMOO_2$. This eventually results in the suppression of resistivity in the entire temperature range. It should be ruled out that the interfacial spins at grain boundaries cause the lower temperature resistivity peak because the grain size of ~3 μm in LCMOP is large enough to ignore them.[12] Second, the postannealing relieves the oxygen inhomogeneity, affording the pronounced reduction of the resistivity peak at lower

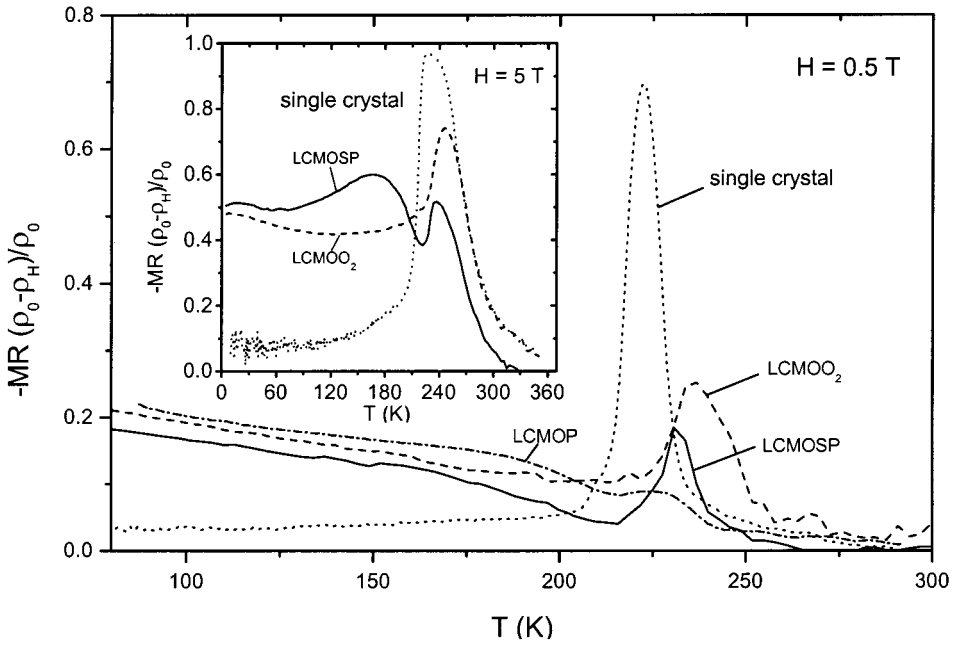

Figure 5. Temperature dependence of magnetoresistance (MR) for all the samples at 0.5 T. The inset presents the MR for $LCMOO_2$, LCMOSP, and a single crystal at 5 T.

temperature.[13] The oxygen incorporation brings about the enhancement of the M−I transition temperature (T_{MI}), which is consistent with that found in the $La_{1-x}Ca_xMnO_3$ film.[14,15]

Figure 4 also shows the MR data for the $LCMOO_2$, LCMOSP, and single-crystal samples. As expected from the double-exchange-type ferromagnetic manganites, the single crystal exhibits large negative MR in the temperature regime near T_{MI}.[16] Unlike this, both polycrystalline samples show the large drop of resistivity with varying field in the whole temperature regimes below T_{MI}. The difference can be seen more distinctively in Figure 5 in which the MR is defined as $(\rho_H - \rho_0)/\rho_0$ where ρ_0 stands for the resistivity at zero magnetic field and ρ_H at certain field. The main panel of Figure 5 shows the MR at 0.5 T, which is relatively in the low-field regime. The overall MR picture for the single crystal in the whole temperature range reveals that the MR change is enormously large near T_C but almost negligible in the low-temperature region. This is true even for the high-field data shown in the inset. Hence, the MR behavior of the single crystal both below and near T_C can be easily understood in terms of the double-exchange framework. Note that the intrinsic MR near T_C is the largest in the single crystal (70% at 0.5 T). In contrast, significant amounts of MR are observed in the polycrystalline materials, $LCMOO_2$ and LCMOSP, in the whole range of temperatures below T_C both in the low- and high-field data. This MR is primarily attributed to the spin-polarized intergranular contribution that originated from the grain boundary effects.[6] A noteworthy feature is that the observed MR peaks in the temperature window of 200−250 K are amplified together with increasing grain size, designating that the intrinsic MR responds to the variation of grain size.[17,18]

The inset of Figure 5 shows the temperature-dependent MR obtained at 5 T, which can be considered the high-field data. The single crystal has the largest MR of 97% near T_{MI}. Two distinctive peaks are observed in the MR of the pulverized single-crystal sample (LCMOSP). We believe that the MR found at near T_{MI} is mainly due to the suppression of spin fluctuation and the other broad MR feature below T_{MI} is governed by the combined effect of oxygen inhomogeneity and spin-polarized tunneling between grains. It is intriguing to note that the MR of the pulverized single-crystal sample (LCMOSP) above T_C is lowered with increasing temperature and finally disappeared near 325 K. On the other hand, both the single crystal and $LCMOO_2$ samples undergo a gradual decrease of the MR above T_C but they still have small negative MR values even at 350 K. The overlap of the MR for the single crystal and $LCMOO_2$ above room-temperature represents the improved connectivity in $LCMOO_2$ by interfacial melting.[19] This enhances magnetic correlation between grains, which facilitates the field dependency on the transport property as observed in the high-field MR above T_C in the inset of Figure 5.

To understand the low-field MR observed in the polycrystalline samples below T_C, we measure the field-dependent resistivity and magnetization of $LCMOO_2$ at selected temperatures in detail. The normalized magnetization (M/M_S) data shown in the top panel of Figure 6 appear to display similar features found in the $M(T)$ curve, where M_S indicates the saturation magnetization. As shown in the bottom panel, however, the normalized resistivity data exhibit different temperature dependencies. Especially in the low-field region below 5000 G, at 10 K there is a sharp drop in the resistivity whereas small changes are made at higher temperatures. It is

(16) Raveau, B.; Maignan, A.; Martin, C.; Herieu, M. *Chem. Mater.* **1998**, *10*, 2641.
(17) Mahesh, R.; Mahendiran, R.; Raychaudhuri, A. K.; Rao, C. N. R. *Appl. Phys. Lett.* **1996**, *68*, 2291.
(18) Snyder, G. J.; Hiskes, R.; DiCarolis, S.; Beasley, M. R.; Geballe, T. H. *Phys. Rev.* **1996**, *B53*, 14434.
(19) Prahan, A. K.; Roul, B. K.; Wen, J. G.; Ren, Z. F.; Muralidhar, M.; Dutta, P.; Sahu, D. R.; Mohanty, S.; Patro, P. K. *Appl. Phys. Lett.* **2000**, *76*, 763.

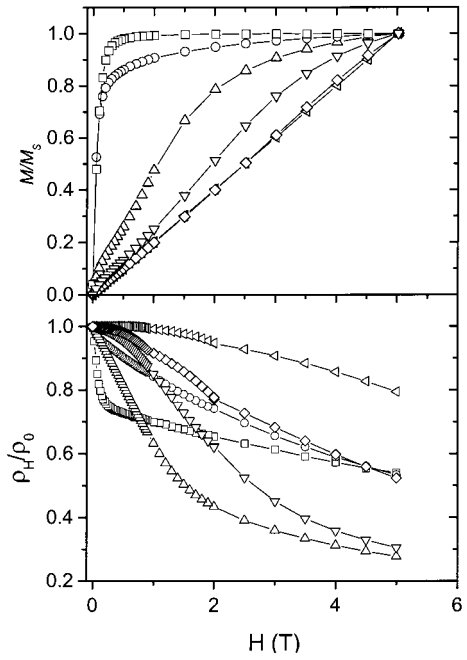

Figure 6. Top panel represents the field dependence of normalized magnetization for $LCMOO_2$ at temperatures of 10 K (□), 215 K (○), 235 K (△), 245 K (▽), 260 K (◇), and 300 K (side triangle). Bottom panel depicts the field dependence of the normalized resistivity.

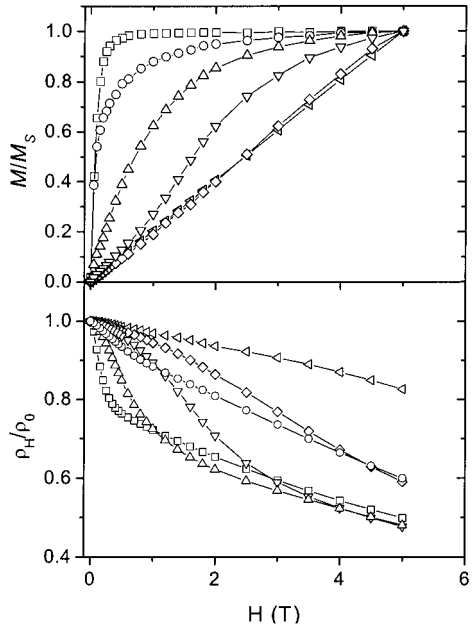

Figure 7. Top panel represents the field dependence of normalized magnetization for LCMOSP at temperatures of 10 K (□), 215 K (○), 225 K (△), 235 K (▽), 250 K (◇), and 300 K (side triangle). Bottom panel depicts the field dependence of the normalized resistivity.

believed that the abrupt suppression of the MR at 10 K in the low-field regime is due to the spin-dependent tunneling at grain boundaries as found in polycrystalline $La_{2/3}Sr_{1/3}MnO_3$ materials.[6] This feature is also found in LCMOSP at 10 K. The magnitude of a low-field resistivity drop of LCMOSP is slightly less pronounced compared to that of $LCMOO_2$, as shown in Figure 7. The MR data of the single crystal without grains shown in Figure 8 would also support our conjecture, in that no appreciable MR change was found

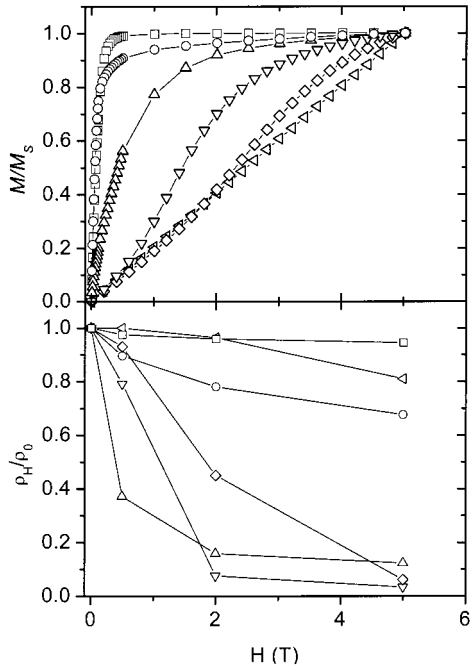

Figure 8. Top panel represents the field dependence of normalized magnetization for the single crystal at temperatures of 10 K (□), 210 K (○), 220 K (△), 230 K (▽), 240 K (◇), and 300 K (side triangle). Bottom panel depicts the field dependence of the normalized resistivity.

in the low-temperature region. Two components emerge simultaneously in the MR curve at 215 K in Figure 6: One is seen as a rapid decrease of negative MR up to about 1000 G and the other as a gradual reduction above that field. The former may be regarded as the effect of spin-dependent granular tunneling and the latter as the blended contribution from intergranular tunneling and the field-induced alignment of disordering spins. The MR is enhanced at high field as the temperature approaches the Curie point because the magnetic spin fluctuation occurring around T_C is suppressed by a magnetic field. Figure 8 shows the field dependence of resistivity and magnetization on the single crystal. The normalized resistivity of the single crystal around T_C behaves like that of $LCMOO_2$, indicating the onset of the field-induced suppression of spin fluctuation.

The MR behaviors found in the $La_{0.7}Ca_{0.3}MnO_{3-\delta}$ materials are basically similar to those observed in the $La_{2/3}Sr_{1/3}MnO_3$ system. However, there are some discrepancies in the MR features, especially in the high-field region. For instance, the MR curves in the $La_{2/3}Sr_{1/3}MnO_3$ system become parallel in the high-field regime below T_C while the $La_{0.7}Ca_{0.3}MnO_{3-\delta}$ samples studied have crossing points of the MR in the same condition. Although the difference is not clearly understood at this stage, our result suggests that the $La_{0.7}Ca_{0.3}MnO_{3-\delta}$ system cannot be simply understood as an extension of the reported $La_{2/3}Sr_{1/3}MnO_3$ work.[6,7]

Conclusions

We have investigated the structural, magnetic, and transport properties of the single crystal of $La_{0.7}Ca_{0.3}MnO_{3-\delta}$ and its polycrystalline congeners with different annealing processes. Their unit cell volumes were not significantly altered but their microstructures were drastically varied depending upon the synthetic path-

way. It is believed that for a polycrystalline sample the presence of grains is the most important factor to determine the magneto transport property. The pulverized single crystal (LCMOSP) straightforwardly accounts for the influence of the grain boundaries on electrical conduction. The magnetization and electrical transport data can be interpreted in terms of the combination of grain boundary effect and oxygen inhomogeneity. The former that renders magnetic transition broader and raises the resistivity background is lessened by interfacial melting while the latter that is likely to produce two peaks in the differential magnetization and resistivity curves is relieved by oxygen annealing at elevated temperature. As expected of the double-exchange ferromagnetic manganite, the single crystal has a large negative MR only at the temperatures near T_C that is mainly due to the suppression of spin fluctuation. The polycrystalline samples exhibit a large MR at low field in the temperatures far below T_C. The low-field MR in $LCMOO_2$ is ascribed to spin-polarized tunneling between grains. This work has clearly demonstrated the granular effects on the MR characteristic of polycrystalline LCMO materials, which will provide an interesting idea to develop low-field MR material.

Acknowledgment. We are grateful to Dr. H. Yi and Dr. H. S. Choi for helpful discussions. We also thank J. O. Lee for measuring the SEM data. The Creative Research Initiative Program financially sponsored this work.

CM0003931